HHS Public Access

Author manuscript

Aerosol Sci Technol. Author manuscript; available in PMC 2024 May 24.

Published in final edited form as:

Aerosol Sci Technol. 2024 March 08; 58(6): 694–705. doi:10.1080/02786826.2024.2322681.

Evaluation of a non-dispersive infrared spectrometer for quantifying organic and elemental carbon in diesel particulate matter

David A. Parks[a], **Yongli Zhao**[b], **Peter R. Griffiths**[c], **Arthur L. Miller**[d]

[a]National Institute for Occupational Safety and Health (NIOSH), Spokane, Washington, USA

[b]Defense Health Agency, Fort Liberty, North Carolina, USA

[c]Griffiths Consulting, San Marcos, Texas, USA

[d]Miller Consulting, Spokane, Washington, USA

Abstract

Diesel particulate matter (DPM) is a common and well-known health hazard in the mining environment. The regulatory method for monitoring both the organic and elemental carbon (OC, EC) portions of DPM is a laboratory-based thermal-optical method with a typical turnaround time of one week. In order to evaluate exposure levels and take corrective action prior to overexposure, a portable real-time device capable of quantifying both OC and EC is needed. To that end, researchers from the National Institute for Occupational Safety and Health (NIOSH) designed and tested the feasibility of a device based on bandpass optical filters that target key infrared wavelengths associated with DPM and its spectroscopic baseline. The resulting device, referred to here as a non-dispersive infrared (NDIR) spectrometer could serve as the basis of a cost-effective, field-portable alternative to the laboratory thermal-optical method. The limits of quantification (LOD) indicate that the NDIR spectrometer can quantify EC, OC, and TC provided they are present at 20, 37, and 46 μg/m^3 or more, respectively. In the event that the NDIR spectrometer is integrated with a sampler and filter tape the LOD is estimated to be reduced to 13, 7, and 10 μg/m^3 for EC, OC, and TC, respectively. These LOD estimates assume a face velocity of 59 cm/s and a sampling time of 30 min.

1. Introduction

Diesel particulate matter (DPM) has been classified as carcinogenic to humans (Benbrahim-Tallaa et al. 2012) and the U.S. Mine Safety and Health Administration (MSHA) regulates

CONTACT David Parks, dparks@cdc.gov, NIOSH, 315 E Montgomery Ave, Spokane, WA 99207, USA.

Disclosure statement

The authors declare there is no Complete of Interest at this study.

Disclaimer

The findings and conclusions in this paper are those of the authors and do not necessarily represent the official position of NIOSH, Centers for Disease Control and Prevention (CDC). Mention of any company or product does not constitute endorsement by NIOSH, CDC.

Supplemental data for this article can be accessed online at https://doi.org/10.1080/02786826.2024.2322681.

DPM exposure with a permissible exposure limit (PEL) of 160 μg/m^3 total carbon over a regular working shift (8 h). Total carbon (TC) is defined as the sum of the organic carbon (OC) and the elemental carbon (EC). Both OC and EC are operationally defined by the NIOSH method 5040, (Birch 2002; NIOSH 2016) which is a thermal-optical method. The use of this method inevitably creates a delay between when the sample is taken and when the analytical results are returned. This delay, typically on the order of one week, in turn creates an opportunity for exposures beyond the PEL to occur and can delay control and remediation efforts.

Portable devices that quantify or estimate DPM in a timelier manner than traditional sampling and laboratory analysis aim to prevent overexposures in the evolving mining environment. For example, the FLIR Airtec can provide 1min temporal resolution. Several devices on the market, including the FLIR Airtec, utilize light absorption or scattering in the ultraviolet (UV) to near-infrared region of the electromagnetic spectrum to estimate DPM. However, these devices are usually estimating black carbon which serves as surrogate for EC.

The fundamental vibrational absorption bands characteristic of the organic carbon in DPM occur in the mid-infrared region of the electromagnetic spectrum (Lin-Vien et al. 1991; Mayo 2004). Since the currently available devices do not interrogate the mid-infrared region of the electromagnetic spectrum, they require aerosol-specific calibrations to accurately quantify both OC and EC (Miller, Habjan, and Park 2007; Watts et al. 2010; Robinson et al. 2014; Northrop, Zarling, and Li 2018; Khan et al. 2020). In this study the % OC in TC was deliberately varied to test a custom non-dispersive infrared (NDIR) spectrometer's ability to quantify all three analytes (EC, OC, and TC) under scenarios which may be encountered in the mining environment. Specifically, this study aimed to emulate scenarios wherein new diesel technologies, including biodiesel and exhaust treatment, are implemented resulting in widely varied EC to OC ratio. Ideally a single calibration would be capable of handling these scenarios, thus this study was designed to evaluate a device which has the potential to accomplish such a task.

Previous work at NIOSH has demonstrated that diffuse reflection Fourier-transform infrared spectrometry (FT-IR) can quantify both the OC and EC fractions of DPM collected on quartz fiber filters (Parks et al. 2021). However, developing a portable and compact real-time monitor for use in workplaces based on current FT-IR technology is challenging and to date has not been accomplished. This study's aim is to evaluate components that could be used in a portable device to quantify OC and EC by way of infrared absorbance. The work reported here demonstrates the application of a simple NDIR spectrometer sometimes referred to as a filtometer (Wilks 2001) based on optical bandpass filters which sample selected regions of the mid-infrared spectrum. These specific regions of the mid-infrared spectrum are the same ones used in Parks et al. (2021).

An NDIR spectrometer can easily be made to possess no moving parts, for far cheaper and can be made much smaller than an FT-IR spectrometer. On the other hand, an NDIR spectrometer has far lower resolution and samples the electromagnetic spectrum at far fewer wavelengths. Lastly, NDIR spectrometers also have the advantage being able to operate

with very high optical speed or low f-number (Wilks 2001). The ability to operate at low-f number implies the commensurate ability to utilize highly focused optics and to benefit from high optical directivity gain.

2. Spectrometer development

2.1. Selection of components

To test the concept of an NDIR spectrometer for quantifying OC, EC and TC within DPM a prototype spectrometer was designed and assembled as shown in Figure 1. The spectrometer is comprised of a broadband incandescent infrared radiation (light) source, five bandpass infrared filters, and a detector. The switching of the bandpass filters was not automated or simultaneous for this benchtop proof of concept, thus, to measure the IR absorption in the narrow infrared passband of each filter, five separate measurements must be taken. For each measurement, the broadband infrared radiation is passed through a bandpass filter, then through a polytetrafluoroethylene (PTFE) aerosol collection filter, before being measured at the detector.

The broadband infrared radiation was generated by an incandescent infrared lamp (HSL-5–115/S Heimann Sensor GmbH). This broadband infrared radiation source was driven by a 5-Volt (115 mA) 5-Hz square wave driver (UPS Driver Vigo System). A thermoelectrically cooled mercury cadmium tellurium (MCT) detector (Vigo System PVI-2TE-4) measured the transmitted infrared radiation that has passed through the DPM collection filter and the optical passband filter. This process is repeated for each of the five pass band filters in turn. The detector output is passed through a preamplifier and on to a 1-MX analog input device (National Instruments USB-6212) where it is averaged over 128 cycles and the peak-to-peak waveform amplitude is recorded. These peak-to-peak amplitudes are rationed to that of the open beam peak-to-peak amplitudes to obtain the transmittance T and then converted to absorbance A by way of $A = -\log_{10}(T)$. The result is a sparse low-resolution absorption spectrum of DPM and the collection filter. Ideally the spectrum of the clean collection filter would be used in lieu of the open beam spectrum to eliminate the variable baseline caused by variable collection filter morphology, however that was not done in this work as will be further discussed in the Section 4.

The particular MCT detector used here was configured with >50% sensitivity over the range from 4000 to 2500 cm^{-1} and >10% sensitivity over the range of 4166 to 2222 cm^{-1}. It is worth noting that MCT detectors can be had which will span all the way down to 303 cm^{-1} however, this is at a cost to sensitivity (Griffiths and De Haseth 2007) and in this study a narrower band detector was chosen to ensure the commensurate increase in sensitivity which resulted in a detectivity of 4.8×10^{11} $cmHz^{1/2}/W$.

A 37 mm diameter 2 μm pore size PTFE aerosol collection filter (SKC 225–1709, SKC, Inc.) was chosen after an evaluation of 25 different collection filter options. This collection filter was chosen due to its lack of fundamental infrared absorption bands above 2500 cm^{-1} as can be seen in Figure 2. Also shown in Figure 2 is the transmission spectrum of the 37 mm diameter quartz fiber filter (SKC 225–317, SKC, Inc.) used in the thermal-optical method NIOSH 5040 and also used in the previously published diffuse reflection mode

infrared spectrometry method (Parks et al. 2021). The Bruker Alpha FT-IR spectrometer used for these measurements was operated in transmission mode and had an effective stray light level of about 2×10^{-4} or (0.02%) transmission. Thus, given absorbance $A = -\log_{10}(T)$ any absorbance greater than about 3.7 can effectively be considered opaque. Further, to allow for a range over which increases in absorbance due to the introduction of an analyte can be accurately measured a limit of 2.5 is prudent. As seen in Figure 2 several spectral regions of the quartz fiber filter exceed $A = 2.5$ including the region from 3000 to 2800 cm^{-1}, which is used for quantifying OC, making this filter not suitable for use in a transmission mode infrared spectrometer intended to quantify DPM. Although the stray light level of the NDIR spectrometer is not known, it is not likely to be less than that of the FT-IR spectrometer and as such this rule of 2.5 or less should be followed.

The selection of the optical bandpass filters (summarized in Table 1) was informed by the FT-IR quantification methods described in Parks et al. (2021). The bandpass filter selection was limited to commercially available off the shelf bandpass filters. Considering this, it is worth noting that custom passband filters can be had and could potentially improve quantification of OC and EC by way of an NDIR spectrometer. Further, as described in the Section 2.2 a simulation can be performed prior to procuring the passband filters. This simulation is detailed in the online supplementary information (SI).

The feature utilized to estimate EC was a monotonically increasing absorption with increasing wavenumber which is likely due to the tail of an electronic absorption band. Specifically, this band is believed to be caused by the promotion of a bonding electron to a nonbonding state. Further, in this case it is suspected to be the $\pi \rightarrow \pi^*$ transition, which peaks in the UV region yet is broad enough that its long wavelength tail affects absorption in the mid-infrared between 4000 and 400 cm^{-1} (Parks et al. 2021). This feature is manifested as a slope in the absorbance. Thus, two bandpass filters were selected to pass wavelengths and therefore measure the infrared absorbance in regions of the spectrum wherein no other significant absorbance bands are present. Additionally, the filters were selected to be far apart in wavenumber thereby ensuring the monotonic increase in absorbance results in a significant difference in absorbance as measured by these two bandpass filters. The two bandpass filters which fit these criteria were one at a relatively high wavenumber of 4049 cm^{-1} and one at a relatively low wavenumber of 2632 cm^{-1}. It is worth noting that 2632 cm^{-1} is the essentially the lower limit of the MCT detector's operating range, otherwise a smaller wavenumber passband would have been chosen, for example in Parks et al. (2021) 828 cm^{-1} was used.

The feature utilized to estimate OC, again based on (Parks et al. 2021), was the set of four overlapping aliphatic C-H stretching bands found between 3000 and 2800 cm^{-1}. These are the aliphatic C-H stretching bands which typically overlap and are due to the symmetric and antisymmetric stretching of CH_2 and CH_3 bonds (see Figure 4). Three bandpass filters were chosen to sample the aliphatic C-H stretching bands, one on either side to obtain a baseline and one encompassing the stretching bands absorbance peaks to quantify them after the baseline correction.

2.2. Prototype spectrometer testing methods

A “sanity check” of the performance of the non-dispersive spectrometer was first performed using polystyrene, a common standard used to calibrate infrared spectrometers, as shown in Figure 3. Figure 3 shows that the non-dispersive spectrometer effectively averages the infrared spectrum over the passband of the bandpass filters. The relationship between the output of the non-dispersive device and the FT-IR spectrum is further expounded upon in the SI. Given the quantitative estimate of the NDIR spectrometers performance provided in the SI and a collection of the relevant FT-IR spectra with the associated known quantities of the analyte in question, a simulation of the NDIR spectrometer’s ability to quantify the analyte in question can be performed. Such a simulation was carried out to confirm the selection of passband filters was suitable prior to obtaining the filter used in this study.

Clearly, considerable spectral information is lost when an NDIR spectrometer is used in place of an FT-IR spectrometer. However, as noted above, the NDIR spectrometer’s bandpass filters were deliberately chosen to collect infrared absorption information germane to OC and EC quantification thereby potentially overcoming the loss in resolution in this context.

When sampling per the method 5040, a quartz fiber filter with an effective area of 8.04 cm^2 is utilized and the mine air is passed through this filter at a rate of 1.7 LPM for roughly 8 h. Given DPM concentrations at the permissible exposure limit (PEL) of 160 $\mu g/m^3$, one would then expect 16 $\mu g/cm^2$ to be deposited on the quartz fiber filter. The deposition of DPM upon the collection filter is effectively uniform (Noll et al. 2005).

Now assume, for the sake of illustration, that the EC/OC ratio is 1; there would then be 8 $\mu g/cm^2$ of OC on the collection filter. To emulate this scenario an aerosol collection chamber and a diesel generator were used as described in (McLaughlin et al. 2020; Parks et al. 2021) to deposit this amount OC per unit area onto a quartz fiber and a PTFE filter using a parallel sampling technique. The deposited OC mass was verified by 5040 analysis on the quartz fiber filter after the spectrum was measured. The assumption was made that the same amount of OC was deposited on the PTFE filter owning to the precision of this parallel sampling technique. The precision of this this parallel sampling technique was quantified over the course of 14 independent experiments and was found to be 3, 8 and 5% for EC, OC, and TC, respectively.

The FT-IR spectra of 8 $\mu g/cm^2$ of OC on the PTFE filter is shown in Figure 4 as is the output of the non-dispersive spectrometer from the same 8 $\mu g/cm^2$ of OC deposited on the same filter. Figure 4 also shows absorption due to the four overlapping aliphatic C-H stretching bands as one would expect for OC in DPM. It can also be seen that in this case the CH_2 band (squares) are more distinct, whereas the CH_3 (diamonds) bands appear faintly as shoulders on the CH_2 peaks.

Figure 4 further shows that the bandpass filter centered at 2916 cm^{-1} had an absorbance above that of the 3077 and 2778 cm^{-1} bandpass filters. This is the desired behavior given the latter are intended for baseline correction and the former is intended to measure the absorbance of the aliphatic stretching bands.

A similar qualitative analysis of the non-dispersive spectrometer's ability to extract spectral information germane to EC was conducted as done above for OC. The analysis was done utilizing the two EC bandpass filters at 4049 and 2632 cm^{-1}, the results of which can be seen in Figure 5. Collection of DPM onto a PTFE and quartz fiber filter again entailed using an aerosol collection chamber and diesel generator as described above. Although an FT-IR spectrum of 8 $\mu g/cm^2$ EC upon the PTFE collection filter was not available, 5 $\mu g/cm^2$ suffices for this qualitative analysis. Again the mass of EC upon the quartz fiber filter was verified by 5040 analysis after the spectrum was measured and this was assumed to be the mass deposited onto the PTFE filter as previously described. The increasing absorbance caused by EC is visible in Figure 5 superimposed upon the monotonic increase in absorbance due to the PTFE filter itself.

Although it was not of consequence here; the FT-IR spectrum was measured first in both evaluations just described. This was not of consequence because both analyses, FT-IR and NDIR, are nondestructive. It was found that the order could be reversed without impact. This was in part owing to the stability of the DPM collected upon the PTFE filter. This stability was confirmed by measuring the FT-IR spectra of nine samples twice with a period of 60 days intervening. A paired t-test was then performed on these FT-IR spectra, which failed the reject the null hypothesis at a significance level of 5% ($\alpha = 0.05$).

3. Materials and methods

3.1. DPM generation and sample collection

The DPM samples used in this study were generated using a diesel generator coupled to a variable resistive load bank as previously described (Parks et al. 2021). The variable resistive load bank alters the ratio of EC to OC affecting a greater relative amount of EC with increasing engine load (McLaughlin et al. 2020). Using a multiport quiescence chamber, parallel samples were drawn through both 37 mm diameter quartz fiber and 37 mm diameter PTFE filters simultaneously to achieve equivalent mass loading. Critical orifices were used to maintain the flow of 1.7 LPM through both filters. The Quartz fiber filter cassettes (SKC 225–317, SKC, Inc.) come equipped with 0.8 μm cut-point impactors whereas the PTFE filter cassettes lacked size selection of any sort. The use of 0.8 μm cut-point impactors is typical because "particles from combustion sources are generally less than 1 μm (diameter)" (NIOSH 2003, 235). This statement is supported by (Noll et al. 2005) in which the laboratory generated samples, when collected without the 0.8 μm impactor, were found to have a mass between 0.4 and 5.7% greater than those collected with the impactor. However, other works have reported greater amounts of supermicron particles of DPM being produced by reentrainment of DPM which had accumulated on the engine cylinder, exhaust system, or in the air sampling system (Kittelson 1998). In any case the PTFE filter cassettes used herein lacked size pre-selection, the implications of which are discussed in the Results and Discussion section below.

A total of 31 PTFE and quartz filter pairs were generated for quantitative analysis. The concentrations within the chamber were higher than that which one would expect to encounter in the mining environment in the interest of accelerating the rate at which DPM samples could be generated. The extrapolation of samples generated in this manner to

samples obtained from a mine environment has been previously evaluated (Parks et al. 2021). The resistive load bank was used to vary the % of OC from one experiment to the next, the variability of the % of OC is summarized in Figure 6 as are the ranges of OC, EC and TC. The range of these values are further described in Table 2.

It should be noted that care was taken to prevent volatile OC from introducing error. Volatile OC has been shown to evolve from the quartz fiber filter rapidly in the first few hours following deposition (Parks et al. 2021). Further the method 5040 is not intended to quantify volatile OC (NIOSH 2016). To prevent the volatile OC artifact the generated samples were left to age for 5days prior to analysis. The evolution of OC from the PTFE filter was investigated in the same manner as was previously done for the quartz fiber filters (Parks et al. 2021) and was found to display a similar although less pronounced trend as shown in Figure 7.

3.2. Infrared analysis and DPM calibration

The DPM deposited on PTFE filters was analyzed using the five-channel NDIR spectrometer. The corresponding parallel samples collected on quartz fiber filters were analyzed using the NIOSH method 5040. The samples were then partitioned into calibration ($N_{calibration} = 20$) and validation ($N_{validation} = 11$) sets using the Kennard-Stone partitioning method (Kennard and Stone 1969) applied to the 2 × 31 matrix of [OC, EC]. The Kennard-Stone partitioning method ensures that the calibration data includes the extremes, thus the validation data is an interpolation as opposed to extrapolation of the developed models. The OC, EC, and TC values as quantified by the method 5040 were then used as the dependent variable and the NDIR spectrometer spectra were used as the predictor variables during calibration. The calibration of the ordinary least squares (OLS) regression models was carried out using the calibration set ($N_{calibration} = 20$) only. The calibrated models are then used to quantify the OC, EC, and TC of the validation set ($N_{validation} = 11$).

4. Results and discussion

This section presents the estimations of EC, OC, and TC produced by OLS regression model applied to the NDIR spectrometer data. The results of the linear regression are shown in Figure 8. It should be noted that in Figure 8 and in general when analyzing filter samples by way of the method 5040 the results are reported as surface density, D, upon the collection filter in μg/cm^2. However, airborne DPM concentrations are quantified in μg/m^3, for example the PEL is 160 μg/m^3 time weighted average (TWA) over an 8-h period.

Conversion of surface density, D upon the collection filter in μg/cm^2, to the more relevant airborne DPM concentration C requires multiplication by a scalar value. This scalar value is a function of the face velocity U_o, and sampling time t as shown in Equation (1).

$$C \times U_o * t = D \quad (1)$$

The face velocity is given by the volumetric flow rate divided by the cross-sectional area of the filter (Hinds 1999). The method 5040 and the associated SKC 225–317 filter cassette utilizes a filter with an 8.04 cm^2 effective area (Noll et al. 2020) and a flow rate of 1.7 LPM (1700 cm^3) for a face velocity of 3.5 cm/s. It is clear from Equation (1) that a higher face velocity results in a higher surface density per unit airborne DPM per unit time. Thus, it is desirable to increase the face velocity to (a) lower the limit of detection (LOD) and or (b) reduce the sampling time required to exceed this LOD.

It has been shown that the face velocity can be increased to 37 cm/s without deleterious effect when using a Pall PTFE filter of unspecified pores size (Noll et al. 2020). As far as commercially available products the very portable (3.8 × 2.4 × 1.0") microAethV® AL30 (AethLabs, San Francisco, CA, USA) utilizes a 3 mm diameter cross sectional area on a PTFE filter at 250 mLPM for a face velocity of 59 cm/s.

To further validate the feasibility of increasing face velocity, the face velocity as a function of back pressure was measured for three of the filters used in the NDIR spectrometer. The results of this test are shown in Figure 9 which indicates that at 59 cm/s a back pressure of 48 in H_2O can be expected. This pressure can be handled for example by the KNF NMP 03 Micro Pump (KNF Neuberger, Inc) while producing a flow of 200 mLPM and consuming 240 mW. Given this information it seems reasonable to assume a face velocity of 59 cm/s and this will be assumed throughout.

Given the assumption of 59 cm/s face velocity a sample rate now needs to be assumed. A rate of one sample every 30 min would be a dramatic improvement over the current thermo-optical laboratory-based method. Further reduction in the sampling time would result in an undesirably high LOD (see Table 4). Therefore, a 30-min sampling period will be assumed. These assumed values for face velocity and sample rate lead to

$$C\left[\frac{\mu g}{m^3}\right] = 9.4 * D\left[\frac{\mu g}{cm^2}\right] \tag{2}$$

The accuracy with which the validation set is quantified is evaluated by way of the coefficient of determination R^2 and the root-mean-square error of prediction (RMSEP) (Kalivas and Gemperline 2006), Equation (3), which are provided in Table 3. It is common to use the term "prediction" as is done in Kalivas and Gemperline (2006) in lieu of "validation" in the context of the initialization RMSEP, however in this study prediction and validation are synonymous. In Equation (3) y_i and $\hat{y}_i$ are the concentration of EC, OC or TC of the ith sample as given by the nondispersive infrared device and the method 5040, respectively, and p is the number of samples in the validation set.

The analogous figures root-mean-square error of calibration RMSEC and coefficient of determination Q^2 apply to the calibration set and are also provided in Table 3. These metrics (Table 3) are derived from the data presented in Figure 8 after scaling each data point by a factor of 9.4. The RMSEC differs from the RMSEP in that the number of degrees of freedom in the model is included in the denominator within the square root as shown in

Equation (4). In Equation (4) y_i and $\hat{y}_i$ are the concentration of EC, OC or TC of the ith sample as given by the nondispersive infrared device and the method 5040, respectively, n is the number of samples in the calibration set and m is the number of coefficients in the regression model (Kalivas and Gemperline 2006).

$$RMSEP = \sqrt{\frac{1}{p}\sum_{i=1}^{p}(y_i - \hat{y}_i)^2} \tag{3}$$

$$RMSEC = \sqrt{\frac{1}{n-m-1}\sum_{i=1}^{p}(y_i - \hat{y}_i)^2} \tag{4}$$

The RMSEC in general is an over optimistic estimate because a portion of the noise in the standards is inadvertently modeled and a better estimate is given by the RMSEP (Kalivas and Gemperline 2006). In other words, typically RMSEP > RMSEC. It is however possible, as in the case for EC here, for the opposite to be true particularly for relatively small sample sizes (Rosa 2010). It is also likely that the EC model in this study would benefit from having more samples in the range of 10 to 15 μg/cm^2 and the data used in this study are a bit biased toward low EC loading.

Another useful metric, the limit of detection (LOD) provides “a decision point used to decide whether to report a significant analyte from the sample.” (Kennedy 1995, p. 65). Provided the data are homoscedastic the variance at the limit of detection will be equal to the variance of blank samples. In this special case the limit of detection can be quantified using the standard deviation of the blank signal (Kennedy 1995) thus:

$$LOD_{estimate} = \mu_{blank} + 3\sigma_{blank} \tag{5}$$

Again, the use of Equation (5) to estimate the LOD requires the data are homoscedastic, which can be verified by way of a Breusch-Pagan. This test provides a quantitative indicator of hetero or homoscedasticity, and is based on the chi-squared distribution (Breusch and Pagan 1979) with the null hypothesis being that the data are homoscedastic. The p-values for this test were 0.1599, 0.4461 and 0.6451 for EC, OC, and TC, respectively, indicating a lack of evidence that the data are heteroscedastic.

To estimate the LOD 17 clean Teflon filters were analyzed for OC, EC and TC with the NDIR spectrometer, the standard deviation and mean of those 17 data were used as in Equation (5) to arrive at the figures provide in Table 4 column 2. The above definition of the LOD may suffice in some cases, however as laid out in Kennedy (1995) a more thorough approach involves using Equation (5) to establish the estimate and then preparing five or

more “low level calibration standards” on spiked sampling media. These standards should span the range of analyte concentrations from less than the LOD to no more than 10*LOD. These standards are used in an additional linear regression, which is not to be confused with the regression performed for the initial calibration. The LOD is then calculated as the three times the standard error, S_y, divided by the slope, m, of this additional regression, as shown in Equation (6).

$$LOD = \frac{3S_y}{m} \tag{6}$$

Note, these “low level calibration standards” must not be included in the original calibration. In our cases these “low level calibration standards” can simply be selected from our validation data set. The LOD is then the largest of

1. Equation (6)
2. The lowest calibration standard
3. The X-intercept if the regression has a negative Y-intercept

For these data, case 1 (Equation (6)) was the largest for all analytes and resulted in the data presented in Table 4 column 3.

Based on Equation (2) these LOD correspond to 2.1, 3.9 and 4.9 μg/cm^2 in Figure 8. This in turn implies that 10 of the samples were below the LOD for EC whereas 4 and 3 samples were below the LODs for OC and TC, respectively. The effect of this can be observed in the relatively large scatter at the low EC range in Figure 8.

It is instructive to notice that the LOD as given by Equation (5) and the RMSEP are not independent in that, assuming homoscedasticity, the RMSEP becomes equal to σ_{blank} in the limit of an infinite number of samples. As such one would expect the LOD to be roughly equal to three times the RMSEP plus the blank filter averages (7, 2, and 9 μg/m^3 OC, EC and TC). This would lead to 25, 56, and 72 μg/m^3 for EC, OC, and TC, respectively. The discrepancy between the RMSEP and the LOD as given by Equation (5) can be attributed, among other causes, to a finite and relatively small number of samples and the fact that the Equation (5) includes none of the variance due to the parallel sampling system or the variance incurred when the parallel samples are analyzed by 5040. That however is not the case for the LOD as given by Equation (6) which does include these variances. However, in Equation (6) S_y is the standard error of the model which produced m in Equation (6). As such S_y is and over optimistic estimate because a portion of the noise in the standards is inadvertently modeled (Kalivas and Gemperline 2006). The over optimistic estimate affects the RMSEC in the same manner. Thus, one could expect that, given a slope m of 1 (the ideal case) and homoscedasticity that that LOD (given by Equation (6)) would be three times the RMSEC plus the blank filter averages giving 31, 47 and 51 for EC, OC and TC. Again, the discrepancy can be attributed, among other causes, to a finite and relatively small number of samples.

The LODs in Table 4 were obtained from multiple collection filters, as were the RMSEP and RMSEC. With this in mind it is illuminating to consider a situation in which a single collection filter is used, and the absorbance of that filter is repeatedly measured as the DPM is deposited. This would be a representative of what is done in the FLIR Airtec or the AL30 aethalometers previously mentioned. In this case the variance in the baseline absorbance due to variable filter morphology is eliminated. To investigate the potential effect this may have on the LOD a single collection filter was analyzed repeatedly in the NDIR spectrometer and Equation (5) was used to estimate this hypothetical LOD which resulted in 13, 7 and 10 $\mu g/m^3$, respectively, for EC, OC and TC.

It should be noted that stretching of the PTFE filter during sampling has the potential to modify the infrared baseline. If this is the case the gains to be had in terms of reduced LOD just described could be subverted. To that end is worth noting that AethLabs has developed unique PTFE filter tape, used in all their aethalometers which does not suffer from this stretching effect. This tape does not suffer from the stretching effect even when utilized, as it is in the AL30, at 59 cm/s face velocity. The infrared spectrum of this filter is provided in Figure 10. Although the absorbance of this filter notably is higher than that of the SKC 225–1709 it is well below the limit of 2.5 previously mention in the Section 2.1.

5. Conclusions

This study provides evidence that an NDIR spectrometer-based monitor could provide the basis for a small portable device capable of quantifying OC, EC and TC in near real-time. This in turn could allow workplace exposure to any and all of these three analytes to be minimized in a timely manner. The ability of the NDIR spectrometer to explicitly quantify OC, EC, and TC within DPM with widely varied % OC in TC translates to improved quantification in the mining environment wherein the % OC in TC can be highly variable. The introduction of next-generation diesel technologies and the use of biofuels is leading to DPM composition showing a significant variability in the % OC in TC compared to that generated by older diesel technologies. Specifically, a 2010 study (Bugarski et al. 2010) showed that when examining diesel emissions with and without a diesel oxidation catalyst and when utilizing either ultralow sulfur diesel, 50% or 100% biodiesel, the % OC in TC ratio ranged from 8.7 to 64.1%. No portable real-time monitors available on the market today can affect the explicit quantification of all three analytes under these conditions and an NDIR spectrometer-based device such as the one investigated in this study could provide a solution. It must be noted that this study was biased toward high OC % in TC samples in an effort to highlight the ability to quantify DPM under such conditions. As a result, more testing of the NDIR spectrometer is needed to evaluate its performance for lower % OC in TC situations, specifically down to 8.7%.

Given that the PTFE filter cassettes used in this study lacked size pre-selection it is possible that the accuracy and precision of the NDIR spectrometer were affected by supermicron particles of DPM. This possibility is feasible in general and more so in this study given the fact that the engine load was varied from, from 3 to 5 kW and it has been shown that varied engine load can affect size distribution of DPM (Cauda et al. 2012). Of particular note, if the DPM particle size approaches or exceeds the wavelength of infrared radiation the scattering

will pass from the Rayleigh scattering regime to Mie scattering regime (Barnett 1942) wherein the scatting behavior varies rapidly with changing particle size. Also of concern is the fact that, if indeed the size distribution was affected by engine loading, the quartz filters which had a 0.8 μm impactor integrated into the cassettes which housed them could have been biased differently during any or each of 31 experiments. Thus, any future works expounding on this study should use the same size selection for both the PTFE and the quartz fiber filter samples. These possibilities do not invalidate this study, but rather provide ample room for improvement and point to potential sources of inaccuracy and imprecision not inherent to the NDIR spectrometry quantification approach itself.

Further work is needed to evaluate the performance of the device when a more diverse set of DPM aerosols is present, for example that from bio-diesels and from a variety of after-treatment equipped diesel engines. This could either reveal weaknesses in the NDIR spectrometer approach or serve to further demonstrate its ability to quantify all three analytes regardless of their relative proportions and regardless of their source.

Another issue that could be addressed in future work is the role of interferants. In the current regulatory method, there is no way to differentiate whether a sample has been contaminated by non-DPM organic compounds. In the mining industry, the assumption is that such compounds are mainly derived from cigarette smoke and oil mist, and the potential interfering effect is minimized by specifying collection methods that avoid the collection of those compounds. The infrared method used in this study will likely suffer from the same issue but there is the possibility that these interferents may not have the same infrared absorbance characteristics.

Supplementary Material

Refer to Web version on PubMed Central for supplementary material.

References

Barnett C 1942. Some applications of wave-length turbidimetry in the infrared. J. Phys. Chem. 46 (1):69–75. doi: 10.1021/j150415a009.

Benbrahim-Tallaa L, Baan RA, Grosse Y, Lauby-Secretan B, El Ghissassi F, Bouvard V, Guha N, Loomis D, and Straif K. 2012. Carcinogenicity of diesel-engine and gasoline-engine exhausts and some nitroarenes. Lancet Oncol. 13 (7):663–4. doi: 10.1016/S1470-2045(12)70280-2. [PubMed: 22946126]

Birch ME 2002. Occupational monitoring of particulate diesel exhaust by NIOSH method 5040. Appl. Occup. Environ. Hyg. 17 (6):400–5. doi: 10.1080/10473220290035390. [PubMed: 12049428]

Breusch TS, and Pagan AR. 1979. A simple test for heteroscedasticity and random coefficient variation. Econometrica 47 (5):1287. doi: 10.2307/1911963.

Bugarski AD, Cauda EG, Janisko SJ, Hummer JA, and Patts LD. 2010. Aerosols emitted in underground mine air by diesel engine fueled with biodiesel. J. Air Waste Manag. Assoc. 60 (2):237–44. doi: 10.3155/1047-3289.60.2.237. [PubMed: 20222537]

Cauda EG, Ku BK, Miller AL, and Barone TL. 2012. Toward developing a new occupational exposure metric approach for characterization of diesel aerosols. Aerosol Sci. Technol. 46 (12):1370–81. doi: 10.1080/02786826.2012.715781. [PubMed: 26361400]

Griffiths PR, and De Haseth JA. 2007. Fourier transform infrared spectroscopy. 2nd ed. Hoboken, NJ: John Wiley & Sons.

Hinds WC 1999. Aerosol technology. New York, NY: John Wiley & Sons.

Kalivas JH, and Gemperline PJ. 2006. Calibration. In Practical guide to chemometrics, ed. Gemperline PJ, 2nd ed. Boca Raton, FL: CRC/Taylor & Francis.

Kennard RW, and Stone LA. 1969. Computer aided design of experiments. Technometrics 11 (1):137–48. doi: 10.1080/00401706.1969.10490666.

Kennedy ER 1995. Guidelines for air sampling and analytical method development and evaluation: US Department of Health and Human Services, Public Health Service, Centers for Disease Control and Prevention. National Institute for Occupational Safety and Health, Division of Physical Sciences and Engineering, 65–7.

Khan MU, Homan KO, Saki SA, Emad MZ, and Raza MA. 2020. Real-time diesel particulate matter monitoring in underground mines: Evolution and applications. Int. J. Min. Reclam. Environ. 35 (4):291–305. doi: 10.1080/17480930.2020.1818937.

Kittelson DB 1998. Engines and nanoparticles: A review. J. Aerosol Sci. 29 (5–6):575–88. doi: 10.1016/S0021-8502(97)10037-4.

Lin-Vien D, Colthup NB, Fateley WG, and Grasselli JG. 1991. The handbook of infrared and Raman characteristic frequencies of organic molecules. London: Academic Press.

Mayo DW 2004. Characteristic Frequencies of Alkanes. In Course notes on the interpretation of infrared and Raman spectra, ed. Mayo DW, Miller FA and Hannah RW, 33–72. New York, NY: John Wiley & Sons, Inc.

McLaughlin R, Parks D, Grubb A, Mason G, and Miller A. 2020. A predictive model for elemental carbon, organic carbon and total carbon based on laser induced breakdown spectroscopy measurements of filter-collected diesel particulate matter. Spectrochim. Acta. Part B Atom. Spectrosc. 168:105871. doi: 10.1016/j.sab.2020.105871.

Miller AL, Habjan MC, and Park K. 2007. Real-time estimation of elemental carbon emitted from a diesel engine. Environ. Sci. Technol. 41 (16):5783–8. doi: 10.1021/es070150a. [PubMed: 17874787]

NIOSH 2003. Monitoring of diesel particulate exhaust in the workplace. In NIOSH manual of analytical methods. 4th ed. Cincinnati, OH: U.S. Department of Health and Human Services, Centers for Disease Control and Prevention, National Institute for Occupational Safety and Health, DHHS (NIOSH) Publication No. 2003–154, https://www.cdc.gov/niosh/docs/2003-154/pdfs/chapter-q.pdf.

NIOSH 2016. Diesel particulate matter (as elemental carbon): Method 5040. In: NIOSH manual of analytical methods. 5th ed. Cincinnati, OH: U.S. Department of Health and Human Services, Centers for Disease Control and Prevention, National Institute for Occupational Safety and Health, DHHS (NIOSH) Publication No. 2014–151, https://www.cdc.gov/niosh/docs/2014-151/pdfs/methods/5040.pdf.

Noll J, Bugarski A, Vanderslice S, and Hummer J. 2020. High-sensitivity cassette for reducing limit of detection for diesel particulate matter sampling. Environ. Monit. Assess. 192 (6):333. doi: 10.1007/s10661-020-8244-z. [PubMed: 32383103]

Noll JD, Timko RJ, McWilliams L, Hall P, and Haney R. 2005. Sampling results of the improved SKC diesel particulate matter cassette. J. Occup. Environ. Hyg. 2 (1):29–37. doi: 10.1080/15459620590900320. [PubMed: 15764521]

Northrop WF, Zarling D, and Li X. 2018. Considerations in using photometer instruments for measuring total particulate matter mass concentration in diesel engine exhaust. J. Eng. Gas Turbines Power 140 (11):112802–5. doi: 10.1115/1.4040306.

Parks DA, Griffiths PR, Weakley AT, and Miller AL. 2021. Quantifying elemental and organic carbon in diesel particulate matter by mid-infrared spectrometry. Aerosol Sci. Technol. 55 (9):1–14. doi: 10.1080/02786826.2021.1917764. [PubMed: 34732970]

Robinson M, Liu ZG, Olson M, and Schauer J. 2014. Comparison of measurement strategies for light absorbing aerosols from modern diesel engines. SAE Int. J. Fuels Lubr. 7 (2):543–50. doi: 10.4271/2014-01-1570.

Rosa GJ 2010. The elements of statistical learning: data mining, inference, and prediction. ed. Hastie T, Tibshirani R, and Friedman J, 219–32. New York, NY: Oxford University Press.

Watts WF, Gladis DD, Schumacher MF, Ragatz AC, and Kittelson DB. 2010. Evaluation of a portable photometer for estimating diesel particulate matter concentrations in an underground limestone mine. Ann. Occup. Hyg. 54 (5):566–74. doi: 10.1093/annhyg/meq020. [PubMed: 20410071]

Wilks P 2001. Infrared filtometers. In Handbook of vibrational spectroscopy, ed. Chalmers JM and Griffiths PR. Chinchester, UK: John Wiley & Sons,.

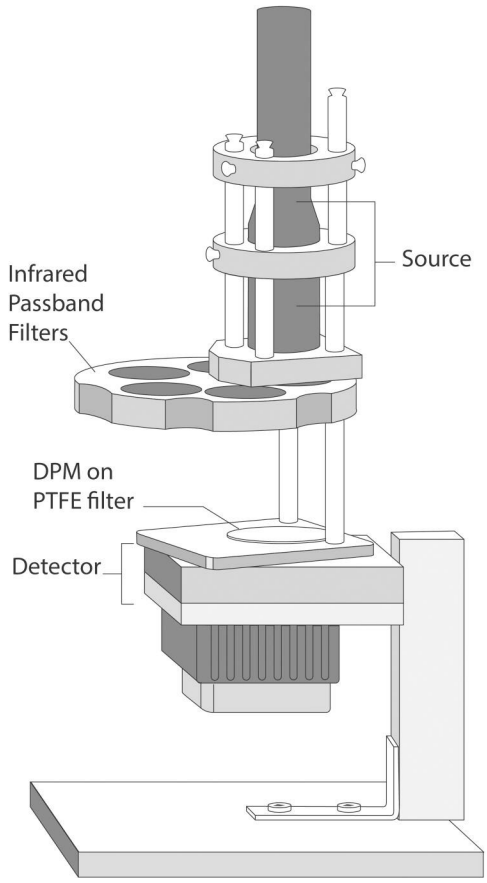

Figure 1.

Schematic of the NDIR spectrometer showing the source. bandpass filters, the aerosol collection filter and the infrared detection module + pre-amplifier.

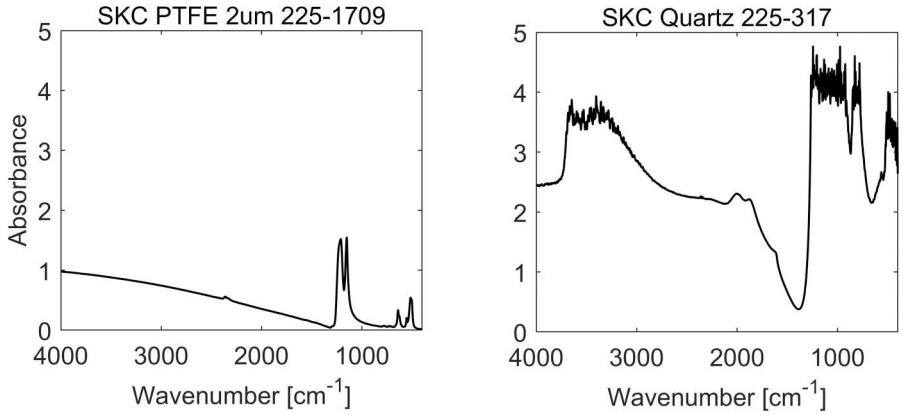

Figure 2.

Infrared absorbance of (left) a clean PTFE aerosol collection filter and of a clean DPM and (right) quartz fiber filter used in the thermal-optical method and the reflection mode infrared spectrometry method. As is the convention in infrared spectroscopy the abscissa is wavenumber in cm^{-1} (that is 1/wavelength). Spectra were measured in transmission mode with a Bruker Alpha FT-IR spectrometer.

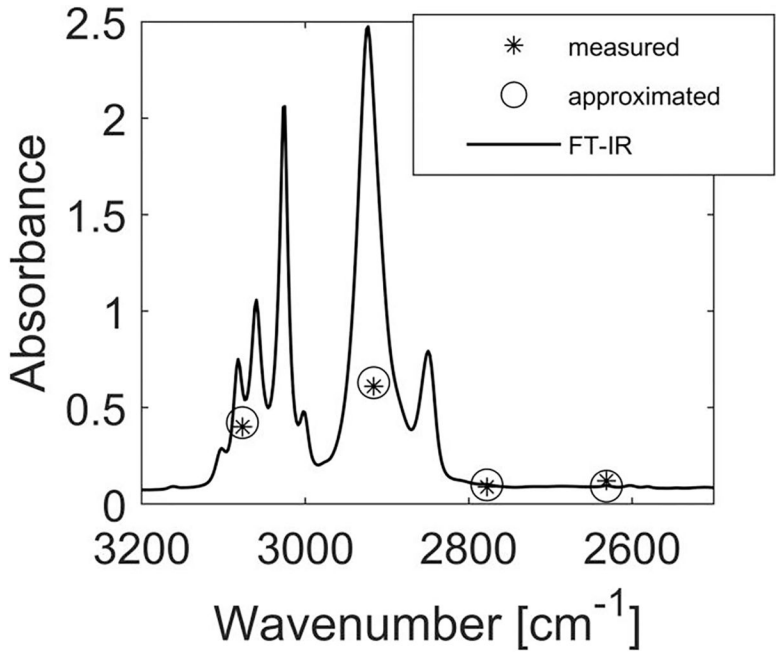

Figure 3.

FT-IR spectrum of a 38-lm-thick polystyrene standard is overlain with the data points measured by the NDIR spectrometer (*) as well as a simulation of the NDIR spectrometer (o). Note that the shortest wavelength sampled by the NDIR spectrometer is not shown here because the FT-IR was configured with an upper limit of 4000 cm⁻1. Spectra were measured in transmission mode with a Bruker Alpha FT-IR spectrometer.

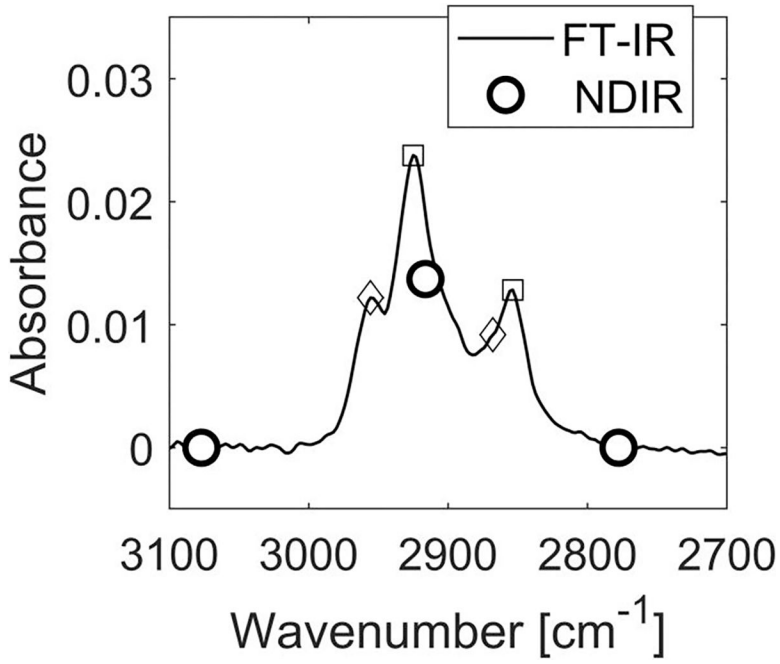

Figure 4.

Aliphatic CH_2 (squares) and CH_3 (diamonds) absorption bands of 8 μg/cm^2 OC on a PTFE filter measured by FT-IR spectrometry and the NDIR spectrometer. FT-IR Spectra have been baseline corrected using a second order polynomial fitted to the spectrum over 3100–3000 and 2800–2700 cm^{-1}. The mass is derived from a parallel quartz fiber filter which was analyzed by the method 5040.

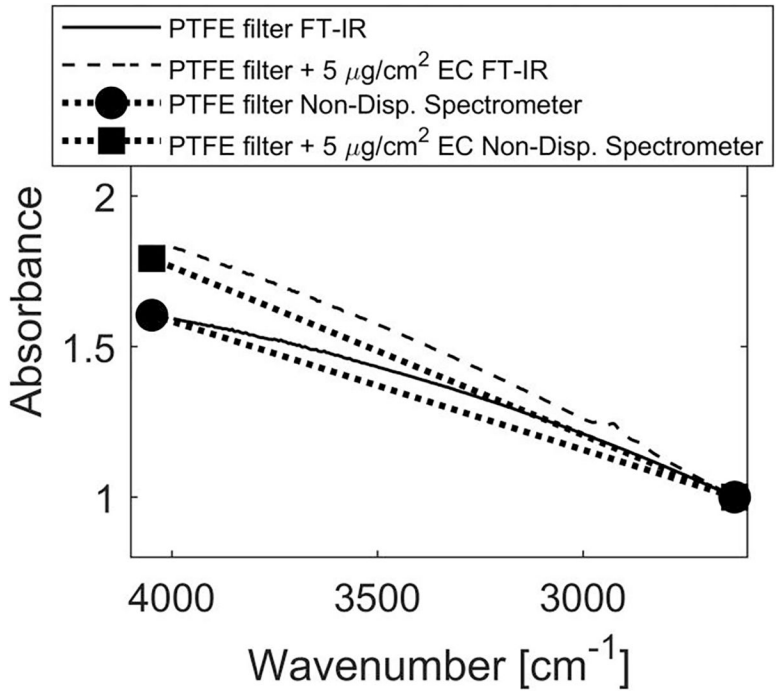

Figure 5.
Sloping baseline associated with DPM EC measured by FT-IR spectrometry and the NDIR spectrometer. All data has been normalized to the absorbance at 2632 cm^{-1} for illustration.

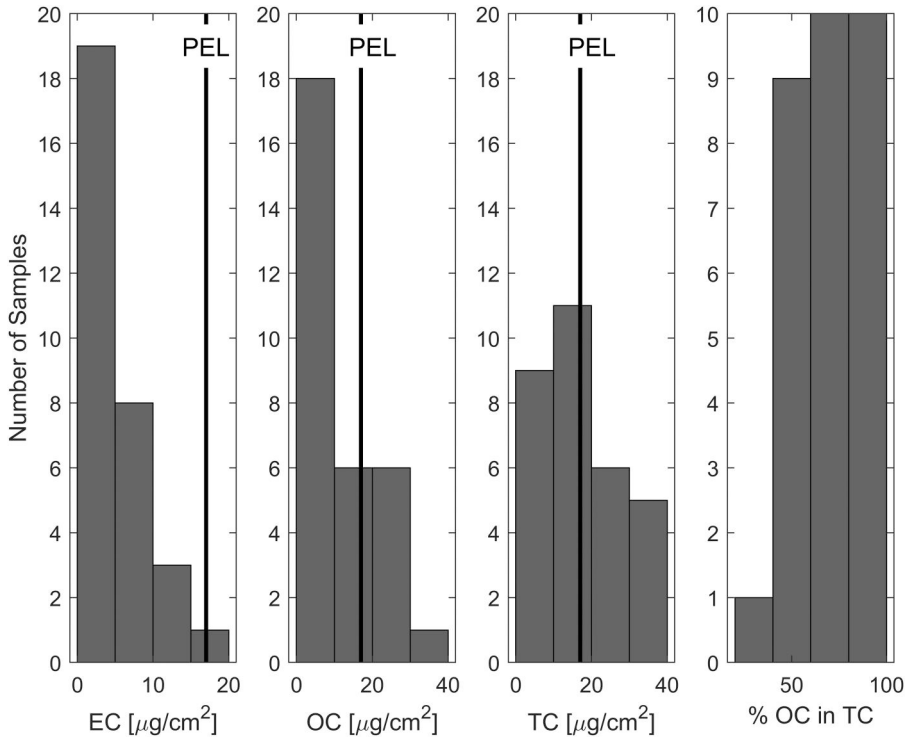

Figure 6.

Summary of the samples used in this study. The solid vertical line represents the PEL if the analyte in question were to compose 100% of the DPM mass. The PEL line is based on a conversion factor from area density to airborne density of 9.4.

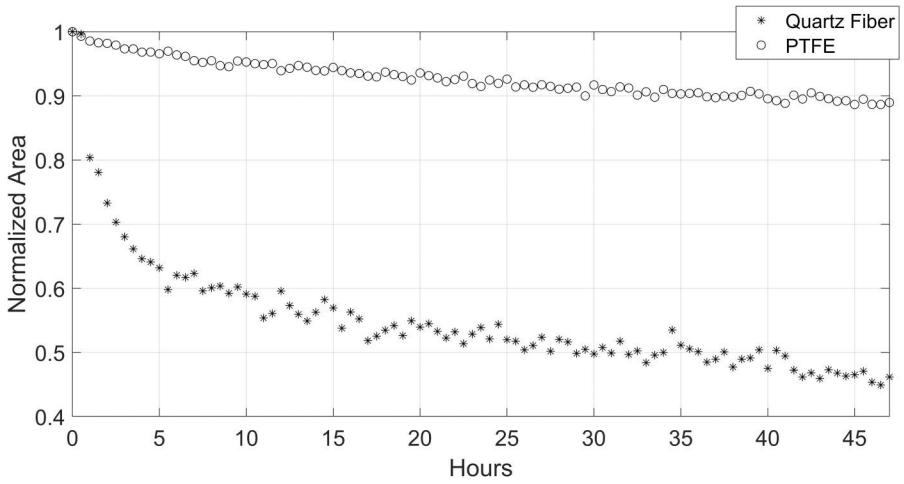

Figure 7.

Integrated area of the aliphatic peaks of a freshly generated DPM sample left at ambient temperature and pressure.

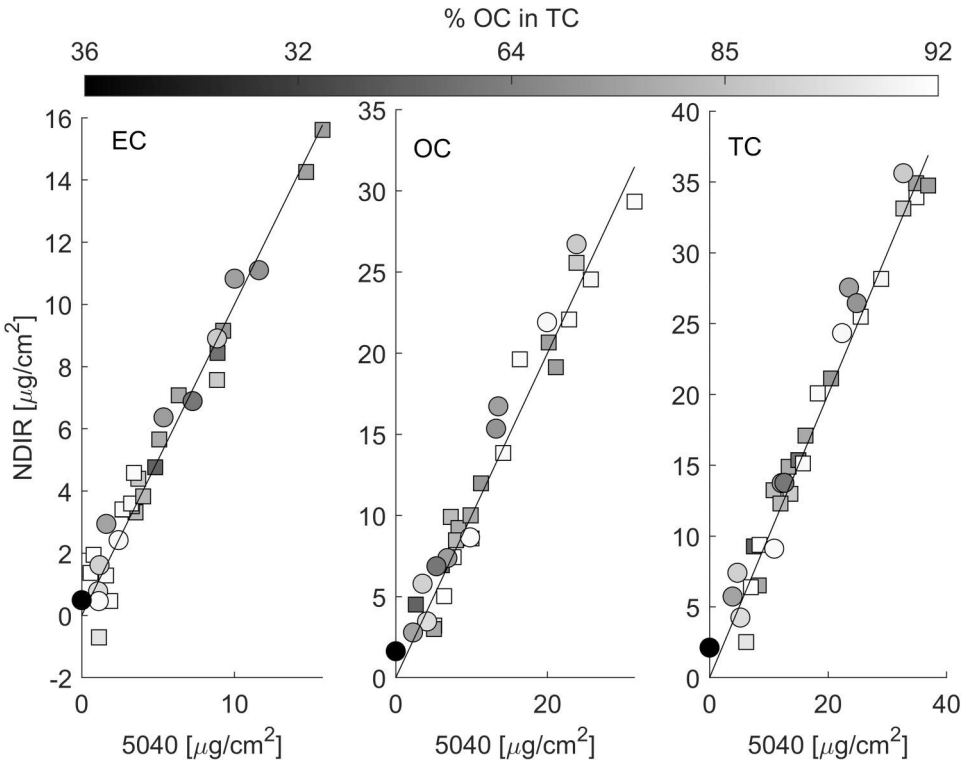

Figure 8.

Graph comparing from left to right the EC, OC and TC as measure by 5040 on the horizontal axis and NDIR on the vertical axis. The solid line is the 1:1 line. Note a conversion to airborne density is possible using a factor of 9.4. The circles represent calibration data and squares represent validation data. Grayscale represents the % OC in TC, note the black circle is a blank sample included in the calibration set.

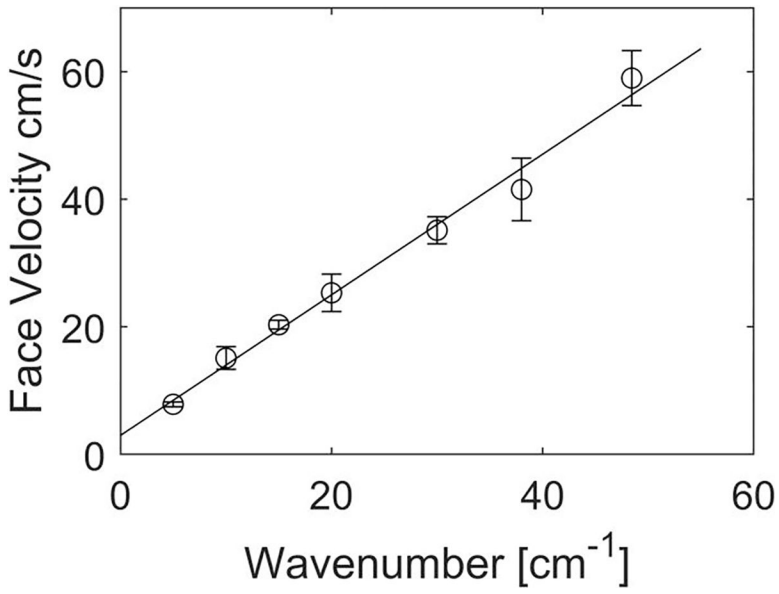

Figure 9.

Back pressure as affected by face velocity for 2 um pore size SKC 225–1709 Teflon membrane filter with cellulose support pad (SKC 225–17). The error bars represent one standard deviation above or below the mean value.

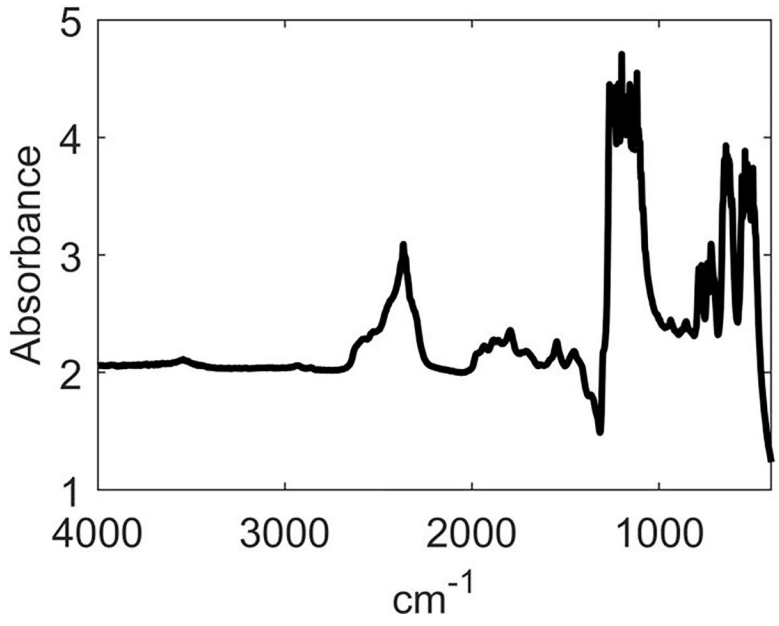

Figure 10.
Infrared absorbance spectrum of the proprietary PTFE filter utilized in the AethLabs aethalometers.

Table 1.

Bandpass filters utilized in the NDIR spectrometer.

Filter center wavenumber (cm^{-1})	Upper half-width wavenumber (cm^{-1})	Lower half-width wavenumber (cm^{-1})	Use
3077	3030	3125	OC baseline
2916	2858	2977	OC absorption
2778	2743	2813	OC baseline
4049	4008	4090	EC absorption slope point 2
2632	2618	2646	EC absorption slope point 1

Table 2.

EC, OC, TC, and % OC in TC for the samples used in this study. Note the results are taken directly form the method 5040 analysis and are thus reported as μg/cm^2 upon the quartz fiber filter.

	EC μg/cm^2	OC μg/cm^2	TC μg/cm^2	% OC in TC
max.	16	31	37	92
min.	0	0	0	36

Table 3.

Root-mean-square error of prediction (RMSEP), coefficient of determination R^2, root-mean-square error of calibration (RMSEC) and coefficient of determination Q^2 assuming a face velocity of 59cm/s and sampling period of 30 min.

Analyte	RMSEP (μg/m^3)	R^2	RMSEC (μg/m^3)	Q^2
EC	6	0.98	8	0.96
OC	18	0.98	15	0.96
TC	21	0.98	14	0.98

Table 4.

Limits quantification assuming a face velocity of 59 cm/s and sampling time of 30 min.

Analyte	Multiple collection filters LOD [μg/m^3] from Equation (5)	Multiple collection filters LOD [μg/m^3] from Equation (6)
EC	25	20
OC	33	37
TC	50	46